CHAPTER 3 FAST ROLL-OFF SINGLE AND DUAL BANDPASS FSSs FOR STEALTH APPLICATIONS*

*Part of this work has been published as:

Venkatesh, G., Singh, S. P., & Thottappan, M. (2024). A novel fast roll-off bandpass frequency selective surface for stealth applications. Journal of Electromagnetic Waves and Applications, 38(5), 571–581. https://doi.org/10.1080/09205071.2024.2321279

3.1. Introduction

Second-order band-pass FSS [84], FSS using V-shaped slots [17], third-order bandpass FSS [85], dual X- / Ka-band FSS [45], bandpass FSS for 5G applications [86], FSS with greater angular stability for RCS reduction [10] have been investigated recently. A bandpass FSS for radome application is presented in [98]. But in all of these designs, observed values of roll-off factor are low (Table 3.4). To get the fast roll-off, the order of the filter, *i.e*. the number of slot arrays should be increased [1]. This is a disadvantage for the bandpass FSS as it would increase the size of the structure. SIW-FSS were used in [99], [100], shorting via array was used in [48], [101], and a 3-D structure was proposed in [102] for fast roll-off but these SIW, shorting via array and 3-D structure increases the complexity of the structure.

In this chapter, a simple low-profile single substrate layer single and dual band bandpass FSSs are investigated through simulation and experimentation, which provides a fast roll-off for stealth applications.

3.2. Proposed Single Band Pass Structure

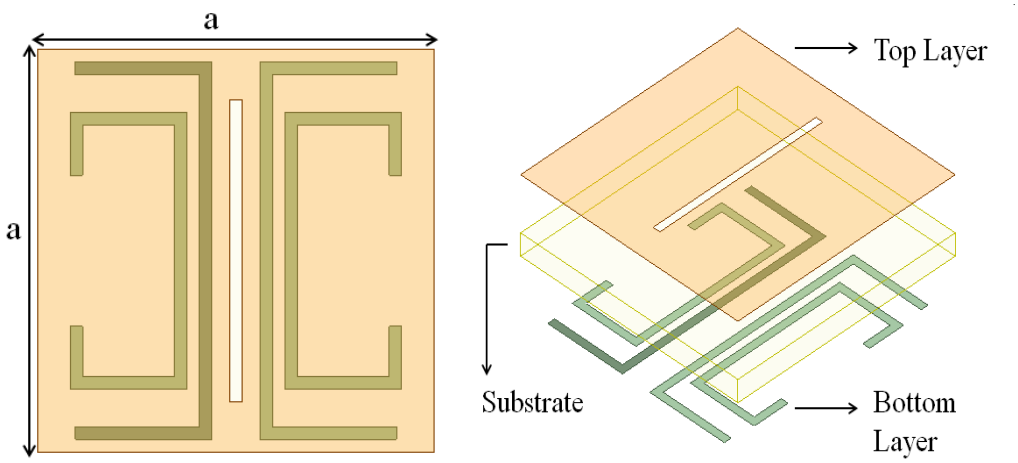

Fig. 3.1 Proposed Structure.

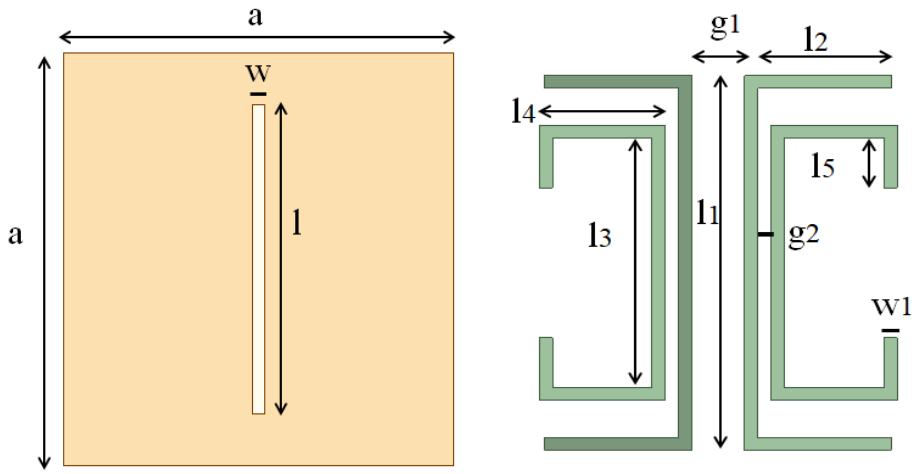

Fig. 3.2. Dimensional parameters of the proposed structure (a) top conducting layer (b) bottom conducting layer.

The proposed FSS unit cell (shown in Fig.3.1) contains a single substrate layer (Number of substrate layers (NSL) = 1) and two conducting layers (Number of conducting layers (NCL) = 2). The dielectric substrate used is RT Duroid 5880 having a thickness (h) of 1.27 mm, relative dielectric permittivity (ε_r) of 2.2, and loss tangent (tan δ) of 0.0009.

Table 3.1 Geometrical Parameter values of proposed FSS Unit cell

Parameter	Value (mm)	Parameter	Value (mm)
a	16	w	0.5
l	12	l_1	15
l_2	5	l_3	10
l_4	4.7	l_5	2
g_1	2	g_2	0.5
w_1	0.5		

The bottom conducting layer (Fig. 3.2) contains two pairs of electric dipoles (resonators) folded at the ends. The electric resonator has a conducting strip. When an electromagnetic wave is incident on the conducting strip and the incoming electric field

is parallel to the conducting strip, the electrons in the conductor move, resulting in the generation of electric current. This electric current causes the conducting strip to resonate at a specific frequency, which depends on the dimensions of the strip. In a periodic structure, at this resonant frequency, the radiated energy from the oscillating electrons in the conducting strip adds in phase with the incoming wave and opposes the transmitted wave. Consequently, at this frequency, the incident wave is completely reflected, and the structure functions as a band-stop filter for incoming electromagnetic waves.

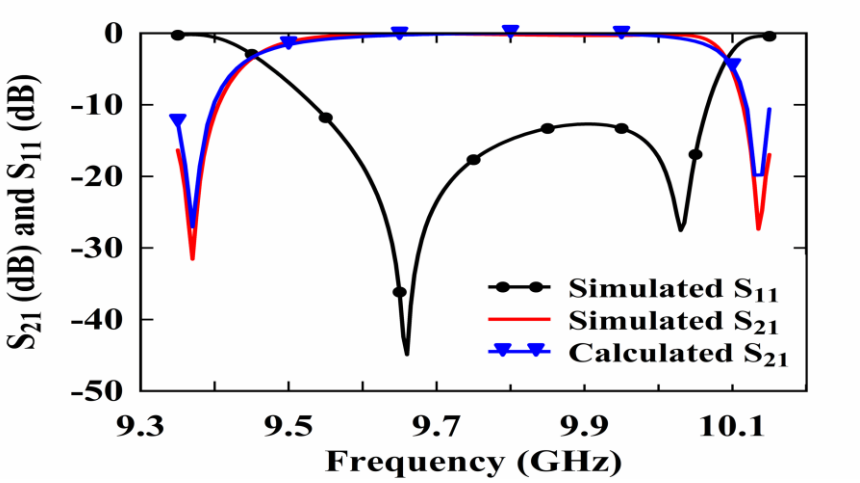

(a)

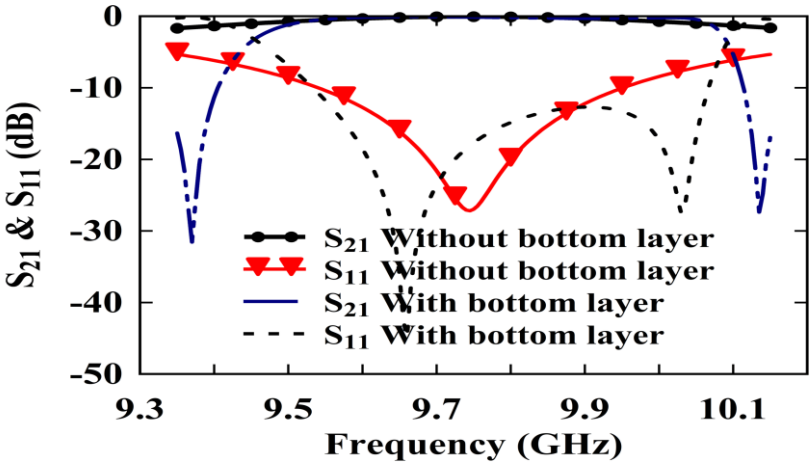

(b)

Fig. 3.3. Simulated frequency response of the structure (a) for TM polarization at normal incidence. (b) with and without bottom layer.

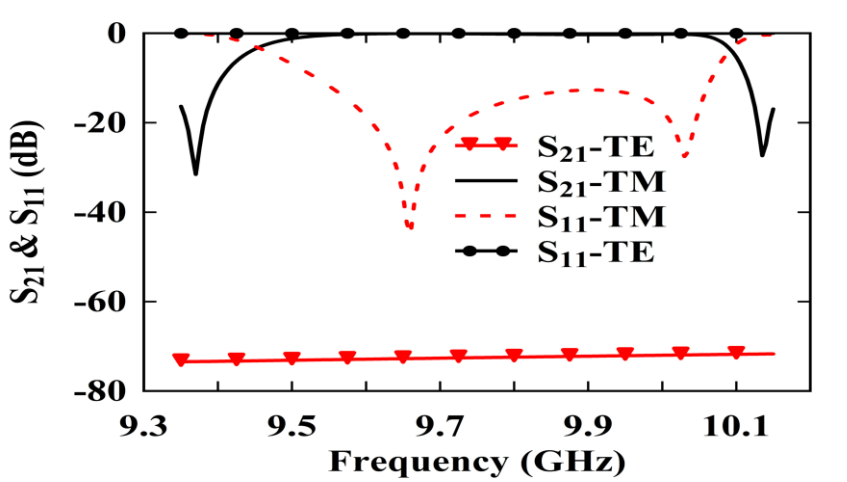

(a)

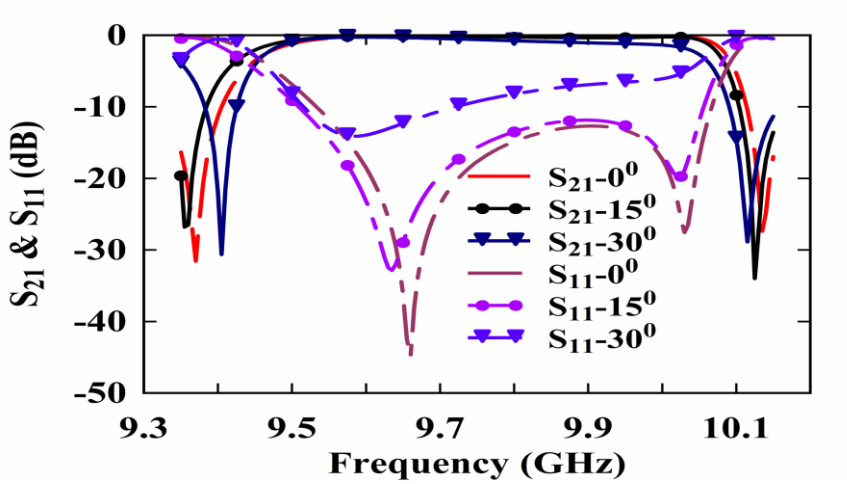

(b)

Fig. 3.4. Frequency response (a) for TE and TM polarizations at normal incidence (b) for different angles of incidence for TM polarisation.

The top conducting layer (Fig. 3.2) of the unit cell contains a vertical magnetic dipole (resonator). The magnetic resonator has a slot on the conducting surface. When an electromagnetic wave is incident on the slot, it induces a voltage in the slot. According to the field equivalence principle, the induced voltage can be represented by a fictitious magnetic current. The slot in the conducting surface is dual to the simple conducting strip (by Babinet's principle). Thus, the structure acts as a band-pass filter for incident electromagnetic waves at a particular frequency, with the frequency depending on the dimensions of the slot. By adjusting two stop-band resonant

frequencies (using two pairs of electric resonators on the bottom conducting layer) to be very close to the two sides of the pass-band resonant frequency (utilizing the magnetic resonator on the top conducting layer), a fast roll-off for the pass-band has been achieved.

The initial dimensions of the structure were estimated using the FSS theory given in [1], where resonance occurs when the length of the strip or slot is approximately half or multiples of half of the wavelength. Subsequently, the dimensions of the structure were optimized using Ansys HFSS software. The optimized dimensions of the proposed FSS unit cell are provided in Table 3.1.

The simulated transmission coefficient-frequency characteristic of the proposed FSS at normal incidence for TM polarization is shown in Fig. 3.3. It can be observed from Fig. 3.3 (a) that the proposed structure functions as a bandpass filter in the X-band of microwave frequencies. Fig. 3.3 (b) Shows the comparison between the transmission coefficient of the structure, with and without the bottom conducting layer. The main drawback of the single conducting layer bandpass structure is its slower roll-off, which makes the spacecraft (aircraft or missile) detectable at the passband edges as antenna of the spacecraft reflects the passband edge signals. By adding two stopbands and adjusting them very close to the two passband edges, a fast roll-off has been achieved, and the spacecraft cannot be detected at the passband edges. The transmission characteristic of the proposed FSS at normal incidence for TE polarization was also studied through simulation, and the simulated characteristic for TE polarization is shown in Fig. 3.4(a) alongside that for TM polarization. Fig. 3.4(a) reveals that a minimum isolation of 40 dB is achieved between the simulated transmission characteristics of the two polarizations. The transmission characteristics for different angles of incidence are depicted in Fig. 3.4(b), where it is observed that only slight

deviations occur in the transmission characteristic when the angle of incidence is varied up to 30 degrees. A slight frequency detuning is observed in the simulated transmission characteristic of the TM-polarized wave for different angles of incidence.

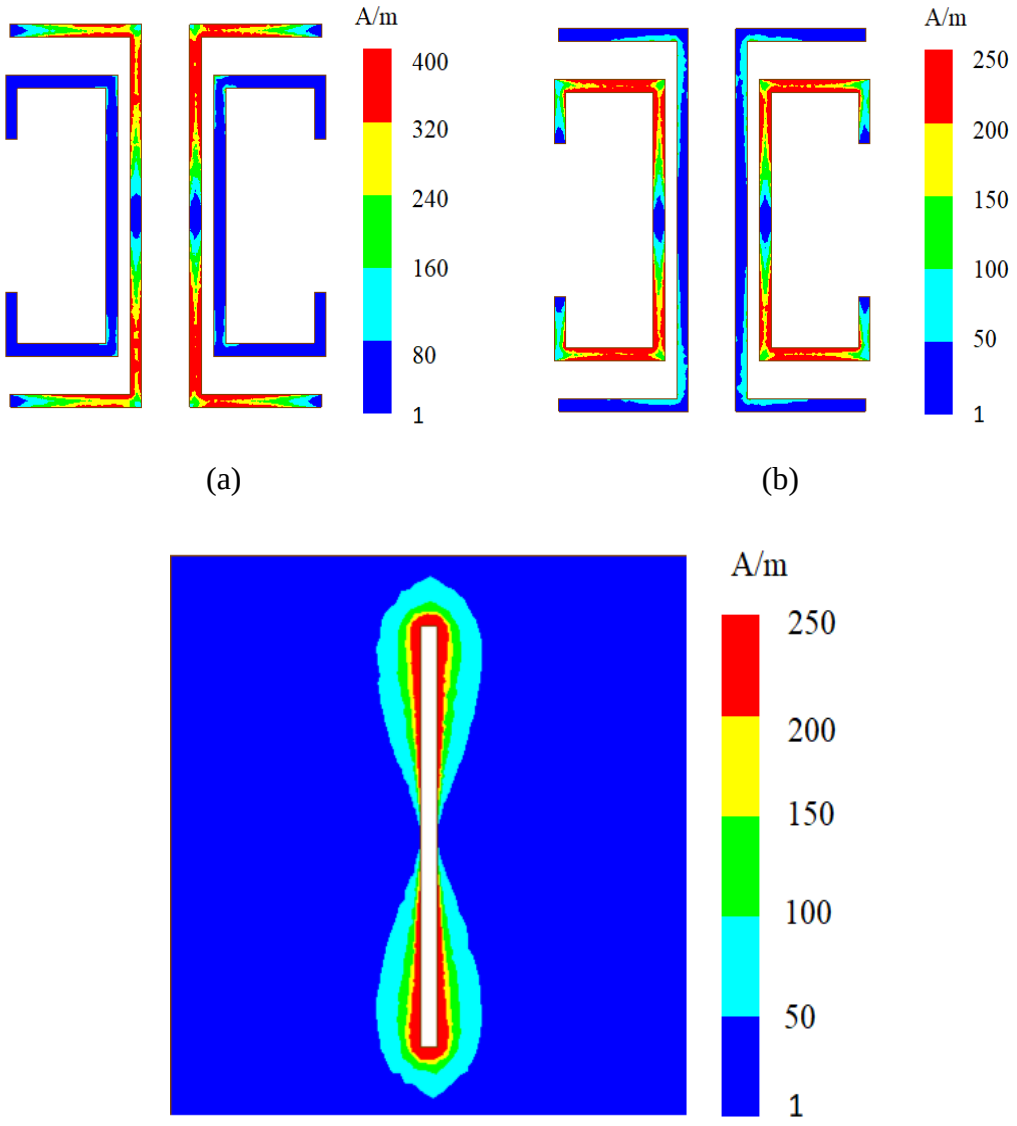

Fig. 3.5. Surface current density plot for (a) the bottom layer at lower stopband resonant frequency (b) the bottom layer at upper stopband resonant frequency. (c) the top layer at pass band frequency.

The resonant behavior of the structure can be understood through the surface current density plots presented in Fig. 3.5. Figs. 3.5(a) and 3.5(b) illustrate the electric

dipoles that contribute to the characteristics of the upper and lower stopbands, respectively. The longer dipole pair corresponds to the lower stopband resonant frequency, while the shorter dipole pair is responsible for the upper stopband resonant frequency. The current density plot at the passband on the top layer of the structure is depicted in Fig. 3.5(c), revealing that the maximum current density is concentrated at the top and bottom edges of the slot.

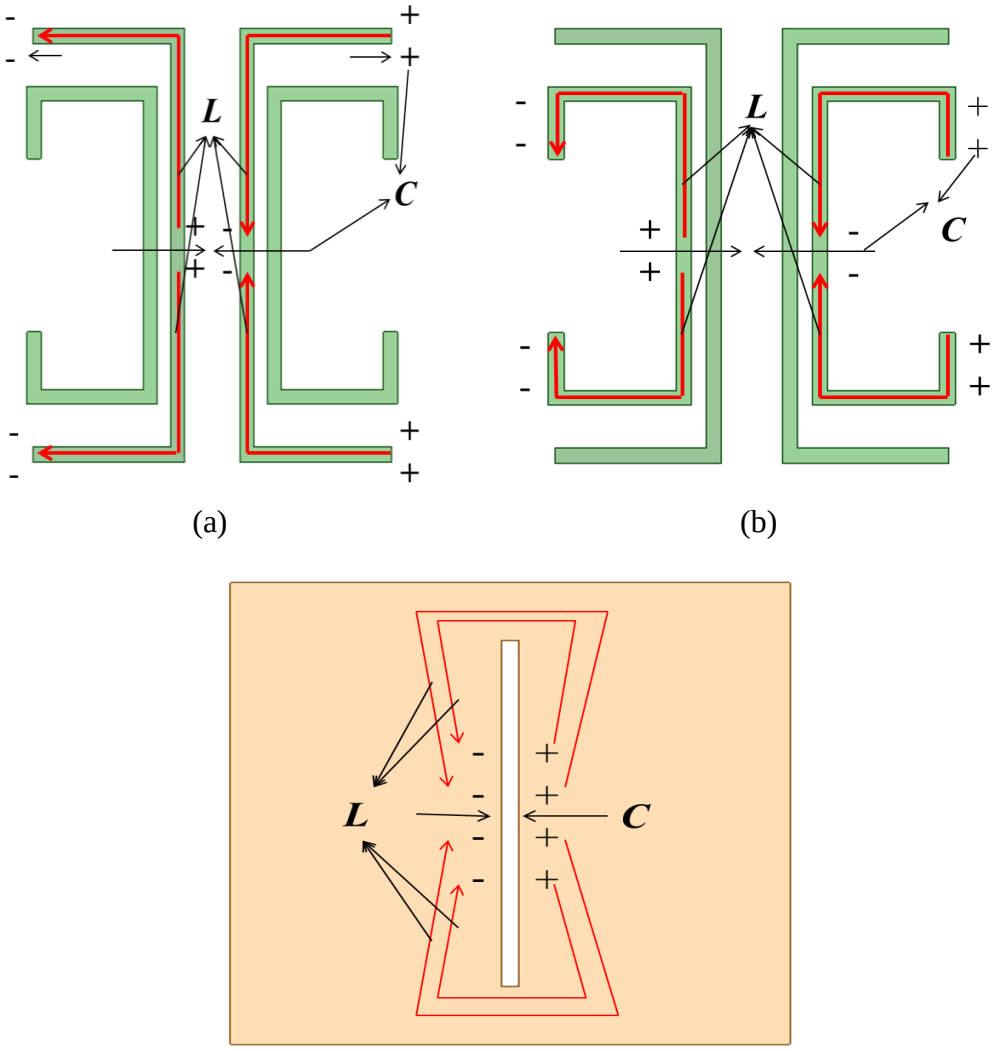

Fig. 3.6. Representation of equivalent circuit parameters for (a) bottom layer at lower stop-band (b) bottom layer at upper stop-band (c) top layer at pass-band.

Table 3.2. Equivalent Circuit Parameters of single bandpass FSS

Parameter	Value (fF)	Parameter	Value (nH)
C_1	150	L_1	1.7728
C_2	1.6	L_2	180.32
C_3	0.8	L_3	308.25

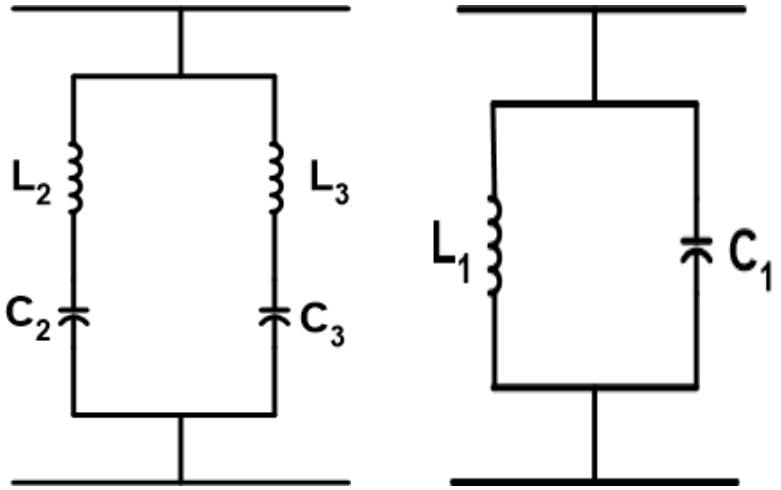

(a) (b)

Fig. 3.7. Equivalent Circuit (a) for the bottom layer (b) for the top layer.

To analyze the structure, the metal patches (dipoles) can be represented by inductors (L2 and L3), while the gaps between the metal strips of the excited dipoles (including coupling capacitance between the layers) can be represented by capacitors (C2 and C3), as shown in Fig. 3.6. The bottom layer can be represented as a parallel combination of two series resonant circuits, as depicted in Fig. 3.7(a). Complementing to the patch array the slot array, on the other hand, can be represented by a parallel resonant circuit, as shown in Fig. 3.7(b), where the slot is represented by the capacitor C1 and the associated excited metal patch is represented by the inductor L1. Using the simulated transmission coefficient (Fig. 3.3), the equivalent circuit parameters (Table 3.2) of the proposed FSS filter were calculated using the procedure given in Chapter 2.

Table 3.3. Frequency Points at Different Transmission Coefficients

S. No.	Lower –N dB frequency point			Upper –N dB frequency point		
	N=3	N=10	N=20	N=3	N=10	N=20
Present Work	9.455	9.405	9.38	10.09	10.115	10.13
[84]	3.56	3.37	2.81	4.03	4.15	4.18
[17]	9.56	9.25	8.75	10.75	11.12	12.25
[85]	7.87	7.75	7.5	9.12	9.25	9.5
[45]	8.75	8.12	7	10.62	10.93	11.5
[86]	24.5	23	21.8	30.25	30.75	31.5
[10]	13.62	12.5	10	15.87	16.25	17
[98]	9.75	9.5	9	10.25	11	11.5
[100]	9.65	9.6	-	10.2	10.25	-
[48]	4.3	4.275	4.25	4.825	4.85	4.875
[101]	9.85	9.8	9.75	10.15	10.2	10.25
[102]	5.7	5.5	5.3	13.5	13.7	13.9
[103]	12.5	11	10.5	19.8	20.5	21
[104]	14	13.7	13.6	16.3	16.4	16.5
[105]	7.25	6.5	6	13.25	13.5	13.75

From Fig. 3.3, the values of -3 dB to -N dB roll-off factor of the proposed FSS for the TM polarization in dB /GHz ($RFL_{N\,dB}$ - lower side of the passband, and $RFU_{N\,dB}$ – the upper side of the passband) are calculated by using,

$$RFL_{N\,dB} = \frac{-3\,dB - (-N\,dB)}{-3\,dB\ frequency\ point - (-N\,dB\ frquency\ point)}$$

$$RFU_{N\,dB} = \frac{-3\,dB - (-N\,dB)}{-N\,dB\ frequency\ point - (-3\,dB\ frquency\ point)} \quad (3.1)$$

Table 3.4. Comparison of the roll-off factor of the proposed FSS with those reported in the literature

S. No	NSL	NCL	RFL 10 dB	RFU 10 dB	RFL 20 dB	RFU 20 dB
Present Work	1	2	140	280	227	425
[84]	2	3	37	58	23	113
[17]	1	2	23	16	21	11
[85]	2	3	58	54	46	45
[45]	2	3	11	23	10	19
[86]	2	3	5	15	6	14
[10]	3	2	6	18	5	15
[98]	3	2	28	10	23	14
[100]	2 (SIW)	3	140	140	-	-
[48]	1 (Via Array)	2	280	280	340	340
[101]	3(Via Array)	4	140	140	170	170
[102]	3 (3-D)	3	35	42	35	42
[103]	1	2	5	9	10	15
[104]	1(3-D)	2	24	43	70	85
[105]	2	3	10	14	28	34
[106]	1(Via)	2	-	154	-	170

The -3 dB, -10 dB, and -20 dB frequency points of the structure for TM polarisation for estimation of simulated roll-off factors are given in Table 3.3 along with the frequency points of FSSs reported in the literature. The values of the simulated roll-off factor for the proposed FSS were determined using Fig. 3.3 and equation (3.1) and the results are compared with the results of FSSs reported in the literature (Table 3.4). The proposed structure offers an improved roll-off factor compared to the structures listed in Table

3.4. Its roll-off factor is comparable to that of roll-off factor of the 3-D and SIW structures, but the proposed structure is simpler than both 3-D and SIW structures, making it easier to fabricate and more cost-effective.

(a)

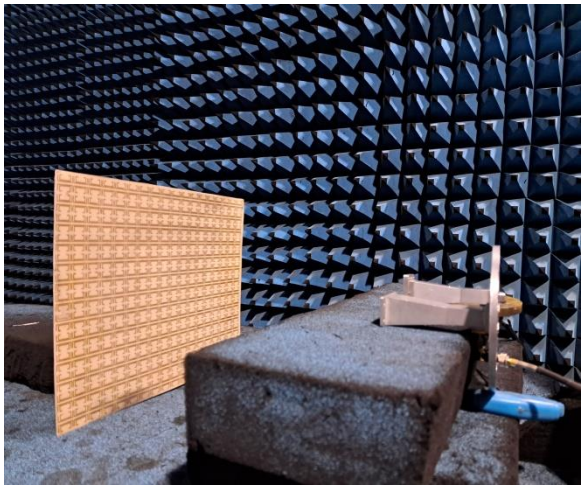

(b)

Fig. 3.8. Measurement setup of the proposed structure for (a) S_{21} (b) S_{11}.

3.3. Experimental Results for proposed single band structure

To verify the simulation performance of the proposed structure, an FSS array consisting of 18 by 13 elements, with an overall size of 288 mm by 208 mm, was fabricated. The magnitude of the transmission coefficient (S_{21}) for the proposed structure was measured in a microwave anechoic chamber, as depicted in Fig. 3.8 (a). The transmission coefficient in the vector network analyzer (VNA) was calibrated by

considering the transmitting and receiving antennas without the structure in the anechoic chamber. To measure the transmission coefficient of the structure (Device Under Test, DUT), the DUT was positioned far away from the transmitting antenna in the far-field region, directly in front of the receiving antenna. The reflection coefficient of the structure measured using the setup as shown in the Fig. 3.8 (b) and VNA calibrated with the same dimensional metal plate.

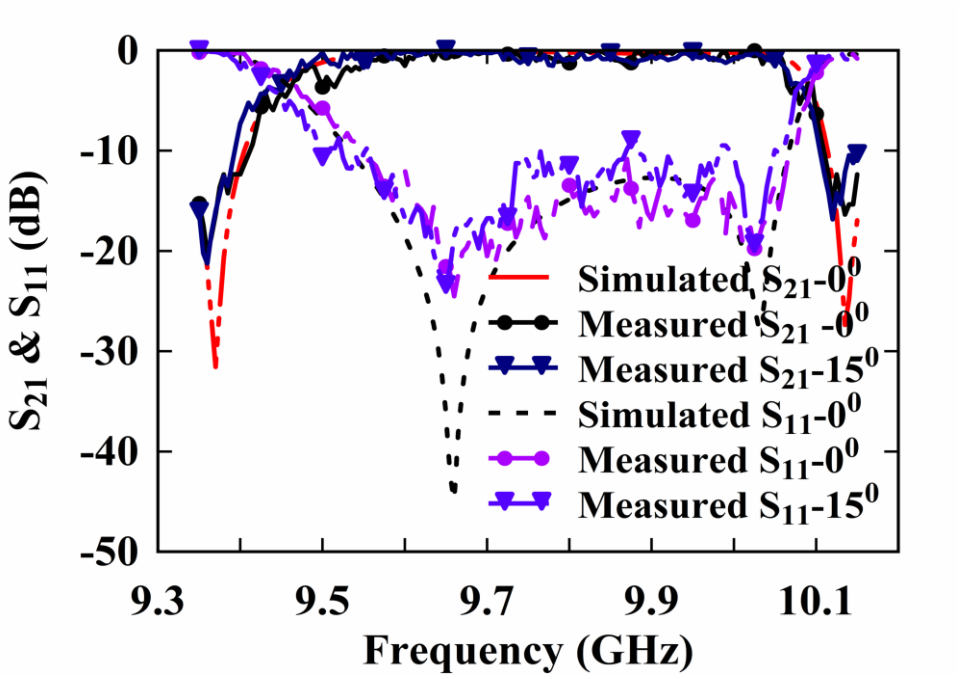

Fig. 3.9. Comparison of measured and simulated frequency response of the structure for TM polarization.

The structure has been designed for single polarization (does not has rotational symmetry). The measured transmission coefficient-frequency characteristic of the proposed array at normal incidence for TM polarization and 15^0 of angle of incidence is presented in Fig. 3.9. At 30^0 of angle of incidence results are deviating from desired response. The measured characteristic of the current array closely agrees with the simulation characteristic (Fig. 3.9). A small deviation between the two characteristics is observed, which can be attributed to fabrication tolerances.

3.4. Proposed Dual Band Pass Structure

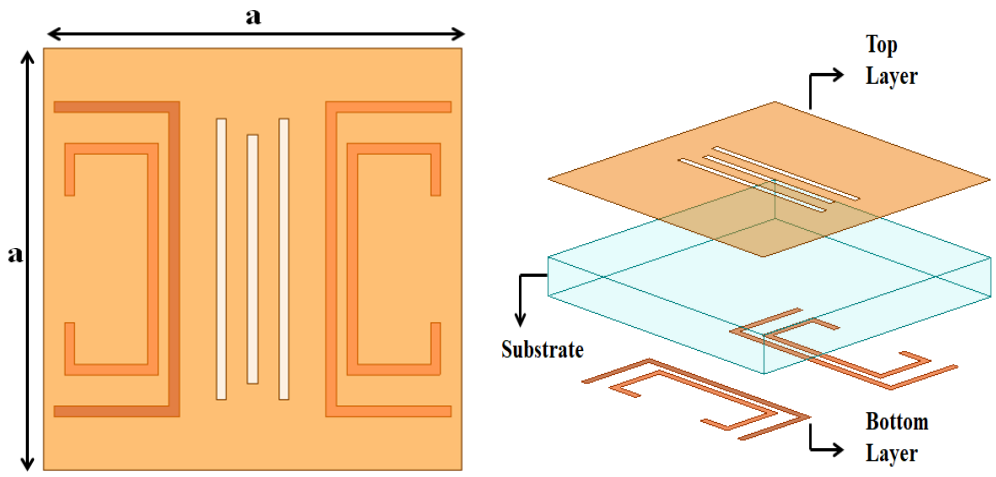

Fig. 3.10. Proposed Structure.

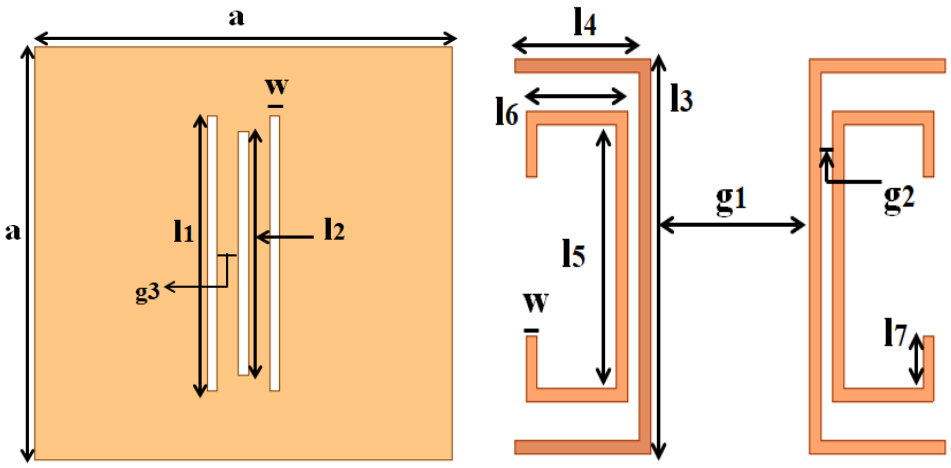

(a) (b)

Fig. 3.11. Dimensional parameters of the proposed structure (a) Top conducting layer (b) bottom conducting layer.

The proposed unit cell for the FSS, depicted in Fig. 3.10, comprises a single substrate layer and two conducting layers. The chosen dielectric substrate is RT duroid 5880 with a thickness (h) of 1.27 mm, relative dielectric permittivity (εr) of 2.2, and a loss tangent (tan δ) of 0.0009. In the top conducting layer (Fig. 3.11), two vertical magnetic dipoles are integrated, responsible for creating the desired passband resonant frequencies for TM polarization, at 9 GHz and 9.735 GHz. On the other hand, the

bottom conducting layer (Fig.3.11) consists of two pairs of electric dipoles, folded at their ends. These two pairs of dipoles yield two stop-band resonant frequencies at 8.605 GHz and 10.195 GHz. The initial dimensions of the structure were estimated based on FSS theory, as outlined in [1]. Subsequently, the structure's dimensions have been optimized utilizing Ansys HFSS software. The resulting optimized dimensions of the proposed FSS unit cell are provided in Table 3.5, signifying the precise configurations achieved for enhanced performance.

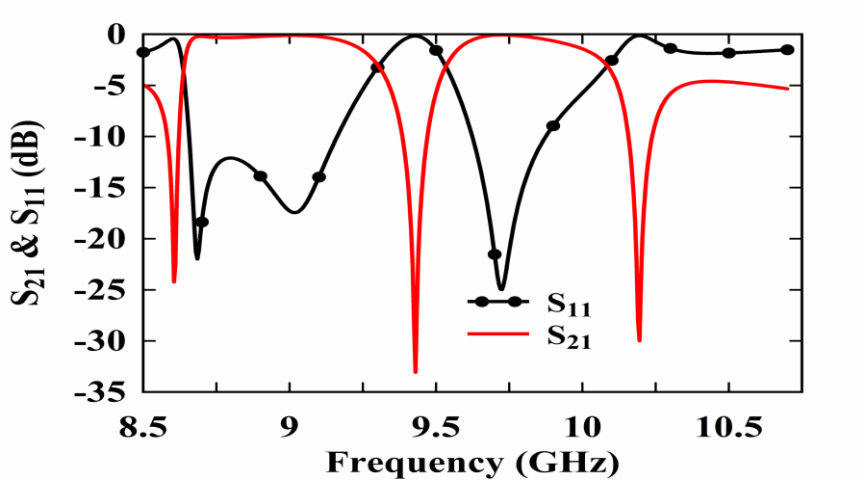

(a)

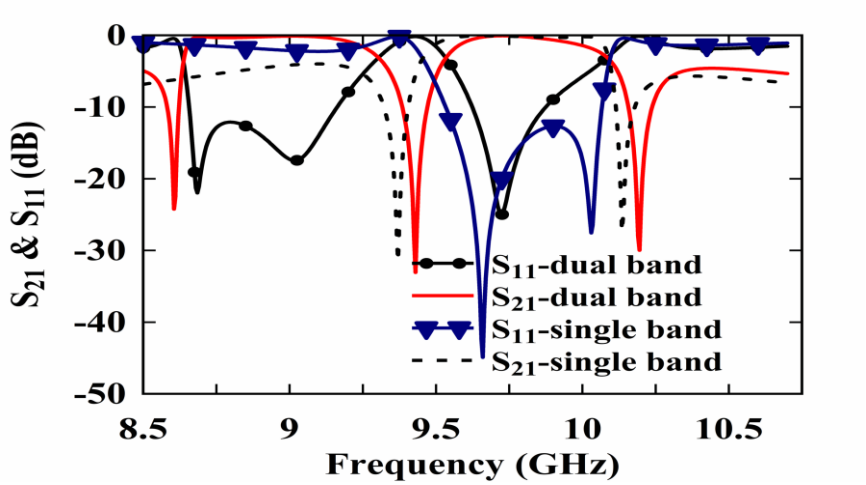

(b)

Fig. 3.12. (a) Simulated transmission and reflection coefficients- frequency characteristic for TM polarization at normal incidence. (b) Comparison of the simulated transmission coefficient of the proposed single and dual band structures.

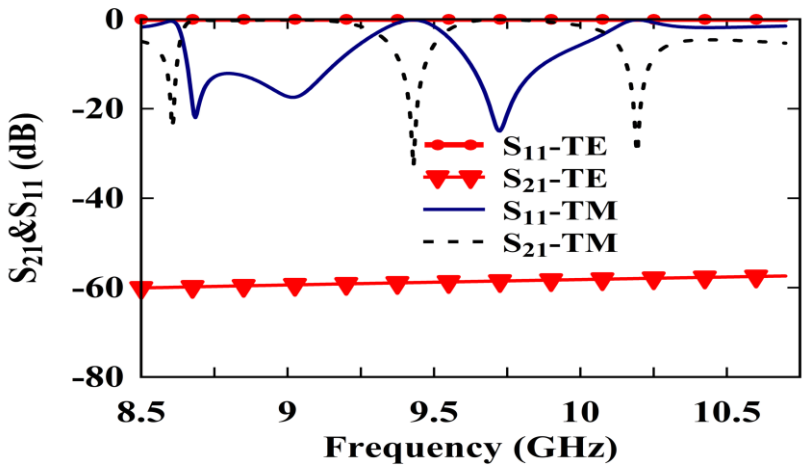

Fig. 3.13. Comparison of the simulated transmission and reflection coefficient of the proposed FSS for TM and TE polarizations.

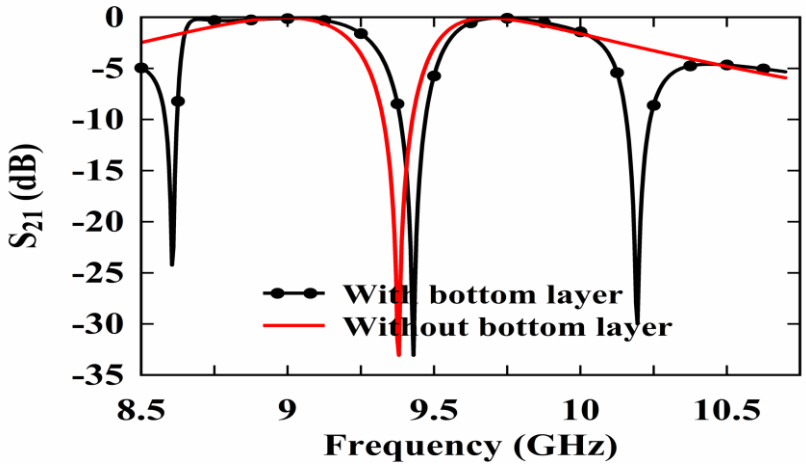

Fig. 3.14. Comparison of simulated transmission coefficient of the proposed FSS with and without bottom layer.

Fig. 3.12 (a) illustrates the simulated frequency response of the proposed FSS when exposed to TM polarization at normal incidence. The graph clearly demonstrates that the proposed structure functions as a bandpass FSS specifically designed for X-band radar frequencies. Comparison of the simulated transmission coefficient of the proposed single and dual band structures is given in Fig.3.12 (b). Additionally, the transmission characteristic of the proposed FSS under TE polarization at normal

incidence has been investigated. The simulation results for TE polarization are presented in Fig. 3.13, alongside the results for TM polarization. It can be observed from Fig. 3.13 that a substantial minimum isolation of 30 dB is achieved between the simulated transmission characteristics of the two polarizations. By adding two electric dipoles on bottom layer the roll-off has been improved (Fig.3.14).

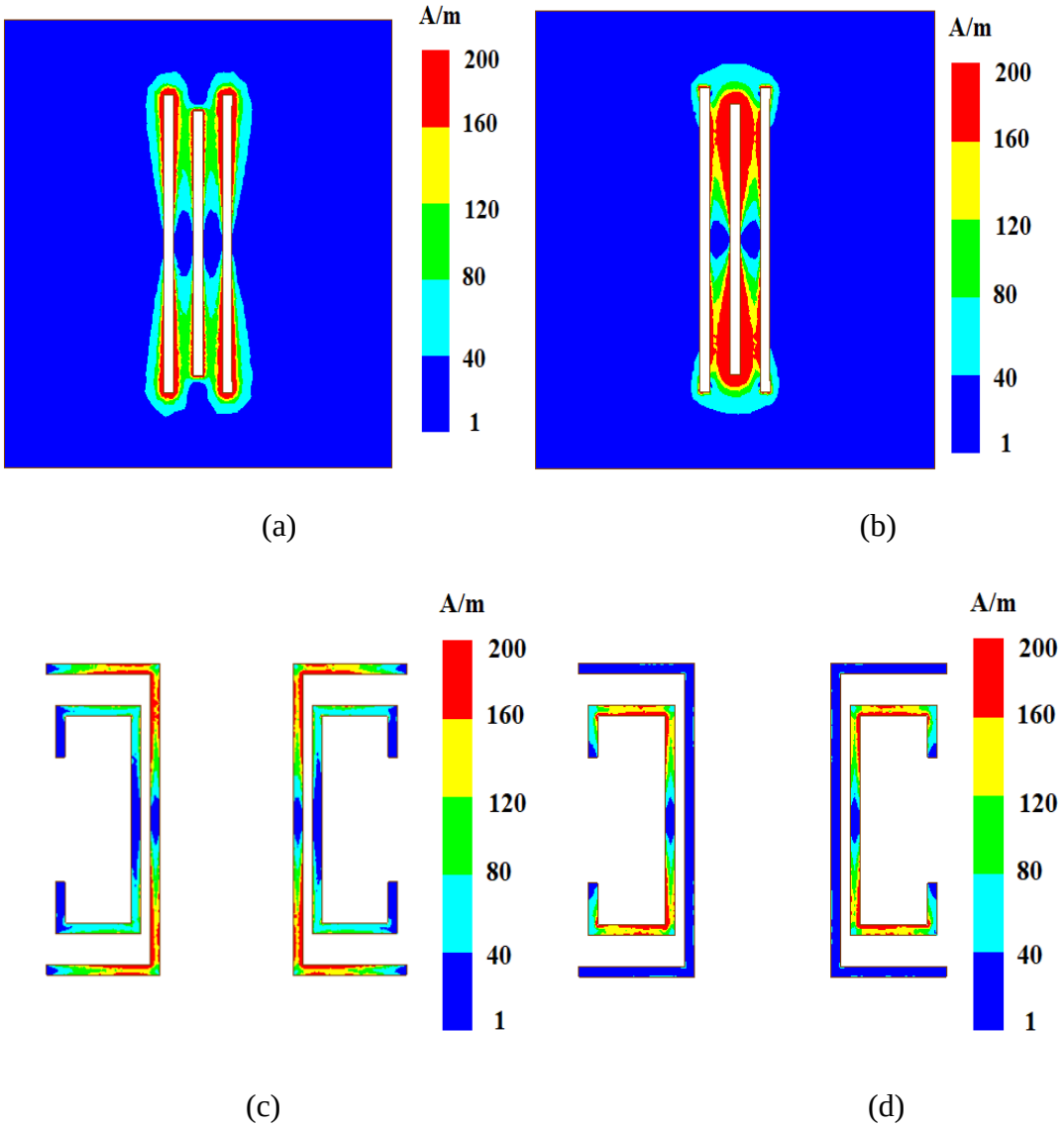

Fig. 3.15. Surface current density plot for (a) top layer at lower pass band frequency (b) top layer at upper pass band frequency (c) bottom layer at lower stopband resonant frequency (d) bottom layer at upper stopband resonant frequency.

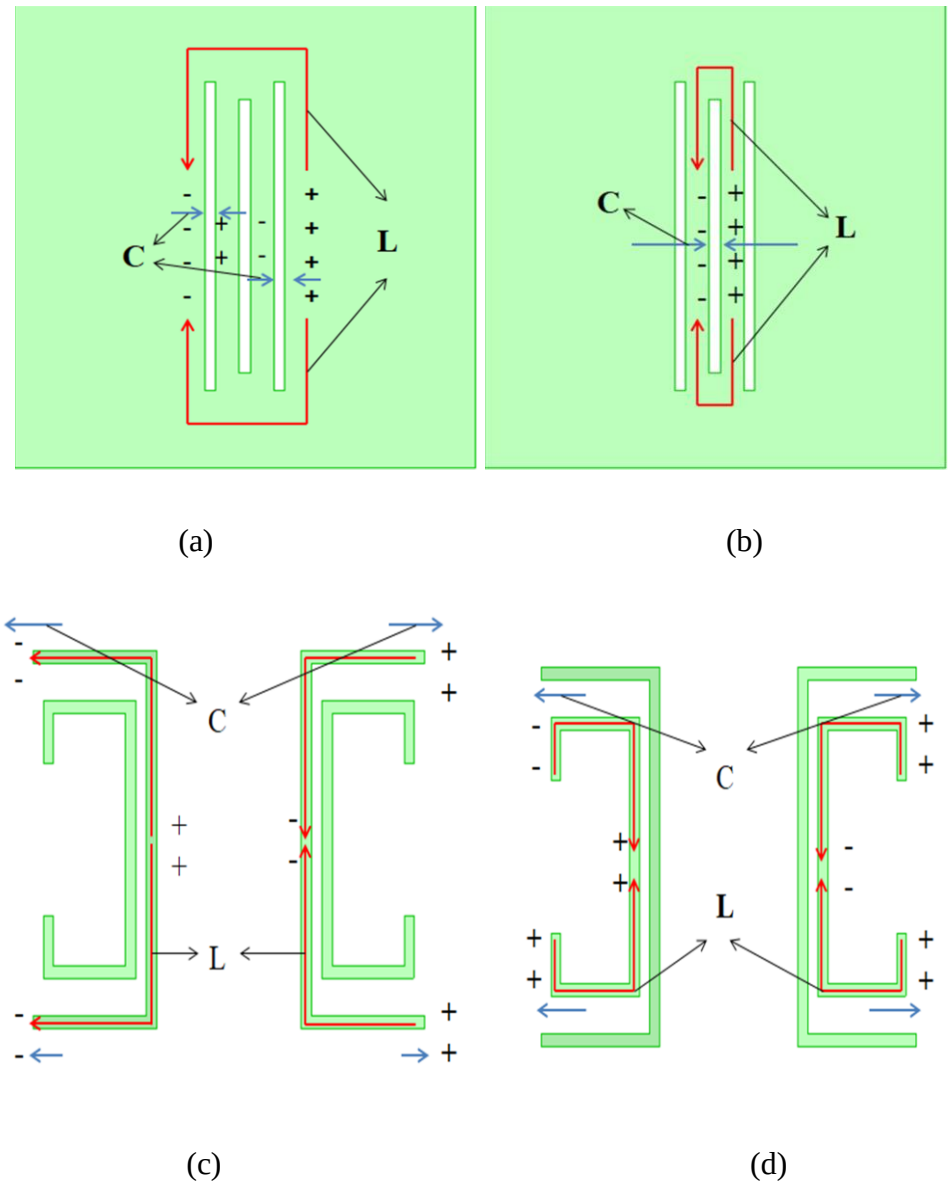

(a) (b)

(c) (d)

Fig. 3.16. Representation of the equivalent circuit parameters for (a) top layer at lower pass band frequency (b) top layer at upper pass band frequency (c) bottom layer at lower stopband resonant frequency (d) bottom layer at upper stopband resonant frequency.

With bottom conducting layer, the transmission coefficient of the structure rises again after reaching lower and upper stop bands but the main drawback of the single conducting layer passband structure has been eliminated. Beyond the passband edges, the transmission coefficient is very low compared to the passband transmission coefficient, so the chance of detecting the spacecraft will be very low.

Table 3.5. Geometrical Parameter Values of Proposed Structure

Parameter	Value (mm)	Parameter	Value (mm)
a	20	w	0.5
l_1	13.3	l_2	11.8
l_3	15	l_4	5.5
l_5	10	l_6	4.5
l_7	2	g_1	7
g_2	0.5	g_3	1

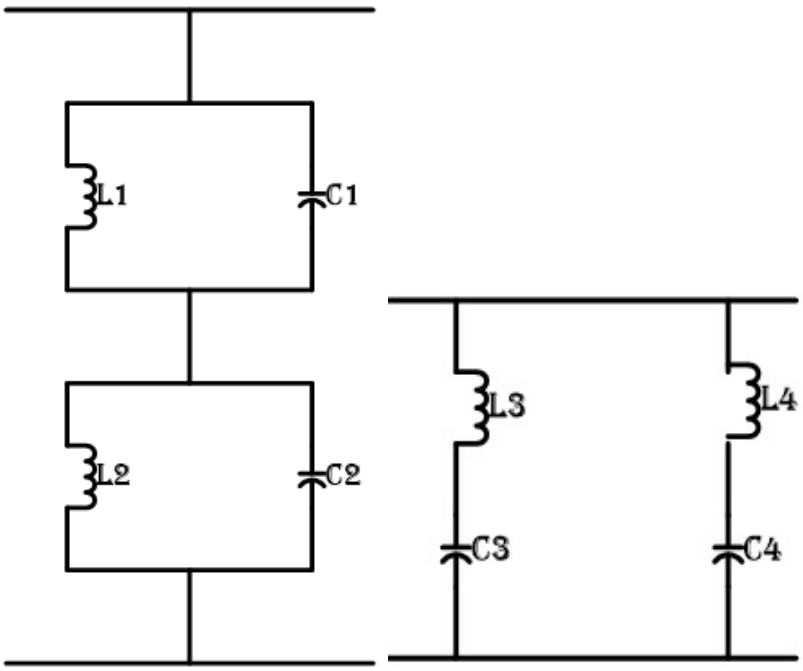

Fig. 3.17. Equivalent circuit (a) for the top layer (b) for the bottom layer.

The resonant behaviour of the structure is elucidated by examining the surface current density plots, as depicted in Fig. 3.15. Fig. 3.15 (a) and 3.15 (b) present the current density plot at passbands on the top layer of the structure. Notably, the maximum current density is observed at the top and bottom edges of the slot, indicating

significant resonant activity. In addition, Fig. 3.15 (c) and Fig. 3.15 (d) reveal the presence of electric dipoles responsible for the lower and upper stopbands, respectively. The pair of longer dipoles is accountable for the lower stopband resonant frequency, while the pair of shorter dipoles contributes to the upper stopband resonant frequency. By analyzing the current density plots, an equivalent circuit of the structure can be derived.

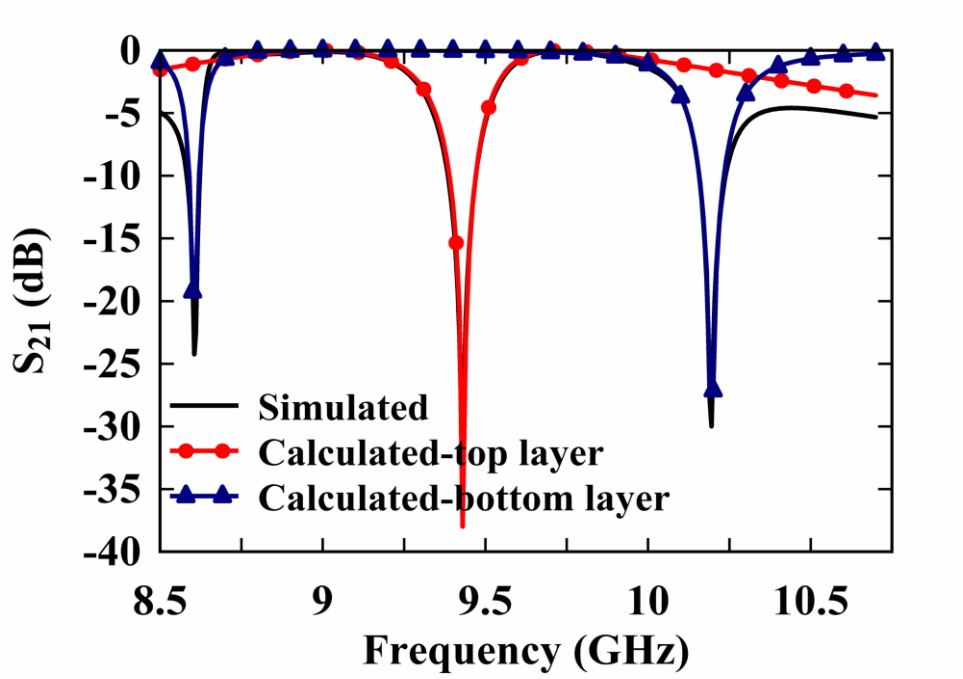

Fig. 3.18. Comparison of simulated and calculated response.

Table 3.6. Equivalent circuit parameters of Dual bandpass FSS

Parameter	Value (fF)	Parameter	Value (nH)
C_1	685.8	L_1	0.456
C_2	937.83	L_2	0.285
C_3	1.03	L_3	332.12
C_4	1.84	L_4	132.45

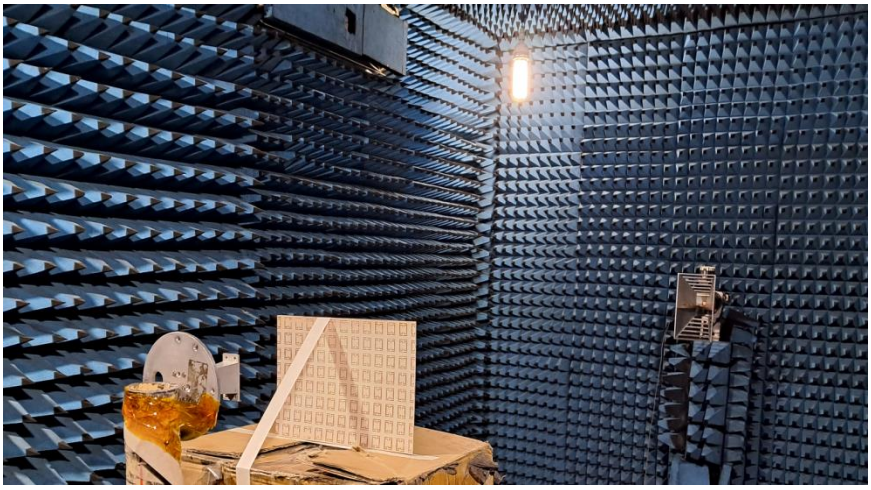

Fig. 3.19 (a). Measurement setup of the proposed structure for S_{21}.

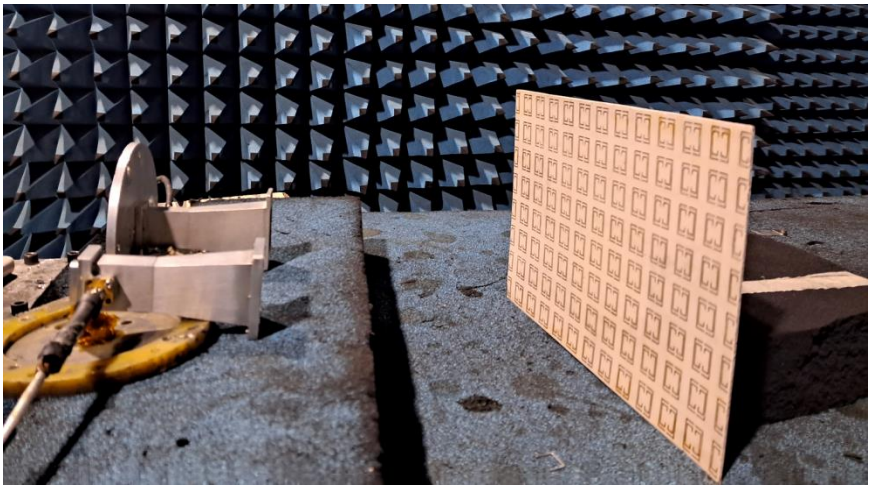

Fig. 3.19 (b). Measurement setup of the proposed structure for S_{11}.

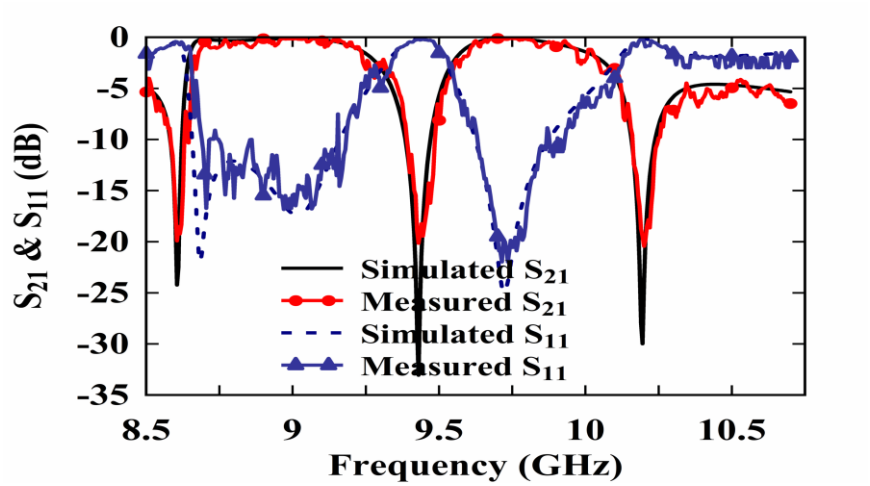

Fig. 3.20. Comparison of measured and simulated transmission results for TM polarization at normal incidence.

The representation of the equivalent circuit parameters is given in Fig.3.16 and this circuit is depicted in Fig. 3.17. With the simulated transmission coefficients, the circuit parameters are calculated using the procedure mentioned in Chapter 2. The equivalent circuit parameters are tabulated in Table 3.6, and the calculated response is presented in Fig. 3.18. This analysis further reinforces the resonant behaviour and functionality of the proposed structure.

3.5. Experimental Results of Proposed Dual Band Pass Structure

In order to validate the outcomes of the proposed structure, FSS array comprising 12 x 08 elements with an overall size of 240 mm x 160 mm has been fabricated. The measurements of S_{21} and S_{11} for the proposed structure were conducted within a microwave anechoic chamber, as illustrated in Fig. 3.19.

The results of the measurements for the proposed array, performed at normal incidence for TM polarization, are illustrated in Fig. 3.20. Remarkably, the measured characteristics of the array closely align with the simulation results shown in Fig. 3.20. However, a slight deviation between the two characteristics is observed, which can be attributed to fabrication and measurement tolerances. Despite this minor discrepancy, the overall agreement between the measured and simulated characteristics affirms the effectiveness and reliability of the proposed structure.

3.6. Conclusion

This chapter presents the design, simulation, fabrication, and experimental testing of a novel fast roll-off single bandpass and dual band pass FSS filters for TM-polarized waves. The proposed structures offer a major advantage in its simple design, which facilitates ease of fabrication with minimal errors. The roll-off characteristics of the proposed single band filter were compared with filters previously proposed in the

literature, and it was found that the present FSS bandpass filter outperformed them. The roll-off factor of the proposed structures are comparable to that of roll-off factor of the 3-D and SIW structures, but the proposed structures are simpler than both 3-D and SIW structures. Therefore, it is expected that the designed FSS structures holds potential as a filter for stealth technology. Furthermore, it was observed that the proposed single band structure exhibited a good response for angles of incidence up to 15 degrees.